

Flexible piezoelectric devices for gastrointestinal motility sensing

Canan Dagdeviren^{1*}, Farhad Javid², Pauline Joe², Thomas von Erlach², Taylor Bense¹, Zijun Wei¹, Sarah Saxton², Cody Cleveland², Lucas Booth², Shane McDonnell², Joy Collins², Alison Hayward², Robert Langer^{1,2,3,4} and Giovanni Traverso^{1,2,5*}

Improvements in ingestible electronics with the capacity to sense physiological and pathophysiological states have transformed the standard of care for patients. Yet, despite advances in device development, significant risks associated with solid, non-flexible gastrointestinal transiting systems remain. Here, we report the design and use of an ingestible, flexible piezoelectric device that senses mechanical deformation within the gastric cavity. We demonstrate the capabilities of the sensor in both in vitro and ex vivo simulated gastric models, quantify its key behaviours in the gastrointestinal tract using computational modelling and validate its functionality in awake and ambulating swine. Our proof-of-concept device may lead to the development of ingestible piezoelectric devices that might safely sense mechanical variations and harvest mechanical energy inside the gastrointestinal tract for the diagnosis and treatment of motility disorders, as well as for monitoring ingestion in bariatric applications.

Systems for sensing of the gastrointestinal (GI) lumen have significantly extended our ability to diagnose and treat patients. Specifically, ingestible electronics have been developed to monitor pH (refs ^{1,2}), manometric pressure³, temperature³, dosage from ingestion to facilitate adherence monitoring³ and even vital signs⁴, as well as for optical imaging in wireless endoscopy⁵. Although these systems have had a significant impact on clinical practice, they are associated with complications, including GI obstruction⁶ and limited battery lifespan, which may impact the completion rates of the evaluation⁷. Recent progress in flexible electronics^{8–12} raises the potential for the development of systems capable of both sensing and remaining flexible, allowing for deformation through the GI tract, potentially mitigating GI obstruction. This advancement could reduce the risk for intestinal obstruction and extend current sensing capabilities by providing systems amenable to implantation for long-term monitoring and/or stimulation. Particularly, active piezoelectric materials^{13–15}, which are more favourable than resistive materials due to their low power, high sensitivity and easy readout features^{16,17}, recent fabrication techniques^{18,19} and associated unusual device structures^{20,21} are helping to advance electronic device integration within the body. Thus, ingestible, flexible electronic devices offer an advanced platform for the diagnosis and treatment of motility disorders, monitoring of ingestion to aid in the treatment of obesity and development of flexible therapies in the form of GI electroceuticals²².

Here, we report the development of a flexible piezoelectric system for monitoring vital signals and ingestion within the GI tract. The device is flexible enough to be folded into an ingestible, dissolvable capsule for delivery. As the capsule dissolves in the GI fluid, the flexible device naturally unfolds and settles on the stomach lining in immediate juxtaposition with the mucosa. The positioning of the device therefore allows for the monitoring of physiological

states of the GI tract. The key findings include in vitro, ex vivo and in vivo demonstrations of a lead zirconate titanate (PZT) GI sensor (GI-S) with output open-circuit voltages (that is, tens of mV) that yielded similar trends, monolithic integration of the sensor with polytetrafluoroethylene (PTFE) hook-up wires and connection to a USB multimeter for simultaneous voltage output recording, and the evaluation of biocompatible forms of the sensor through in vitro cell culture as well as in a large animal model approximating human GI anatomy. Additional results demonstrate the mechanical and electrical stability of the device behaviour over 10,000 cycles of bending and unbending with a moist, ex vivo tissue, and quantitative analytical models that couple the mechanical deformations and piezoelectric effects to predict electrical output as a function of key design parameters, material properties and GI conditions. Collectively, the reported experimental and theoretical findings provide instantaneous information on ingestion states in the GI tract. These developments could help inform a broad range of systems, including devices with the capacity to power gastric resident and implantable systems, as well as sensors applying the instantaneous measurements to sense ingestion and GI motility to guide optimal therapeutic interventions.

Results

Fabrication and design. A PZT GI-S on a glass cylinder shown in Fig. 1a displays the system flexibility to conform to a curvilinear surface. Corresponding schematic illustrations of an individual PZT ribbon and an associated cross-sectional view of the ribbon are shown in Fig. 1b,c, respectively (see Methods). A PZT GI-S comprises 12 groups of PZT ribbons connected in series, where each group consists of ten PZT ribbons connected in parallel⁸. The entire module is encapsulated with a 1.2- μ m-thick layer of

¹Media Lab, Massachusetts Institute of Technology, Cambridge, MA 02139, USA. ²David H. Koch Institute for Integrative Cancer Research, Massachusetts Institute of Technology, Cambridge, MA 02142, USA. ³Department of Chemical Engineering, Massachusetts Institute of Technology, Cambridge, MA 02139, USA. ⁴Institute for Medical Engineering and Science, Massachusetts Institute of Technology, Cambridge, MA 02139, USA. ⁵Division of Gastroenterology, Brigham and Women's Hospital, Harvard Medical School, Boston, MA 02115, USA. *e-mail: canand@media.mit.edu; gi_lab@mailworks.org

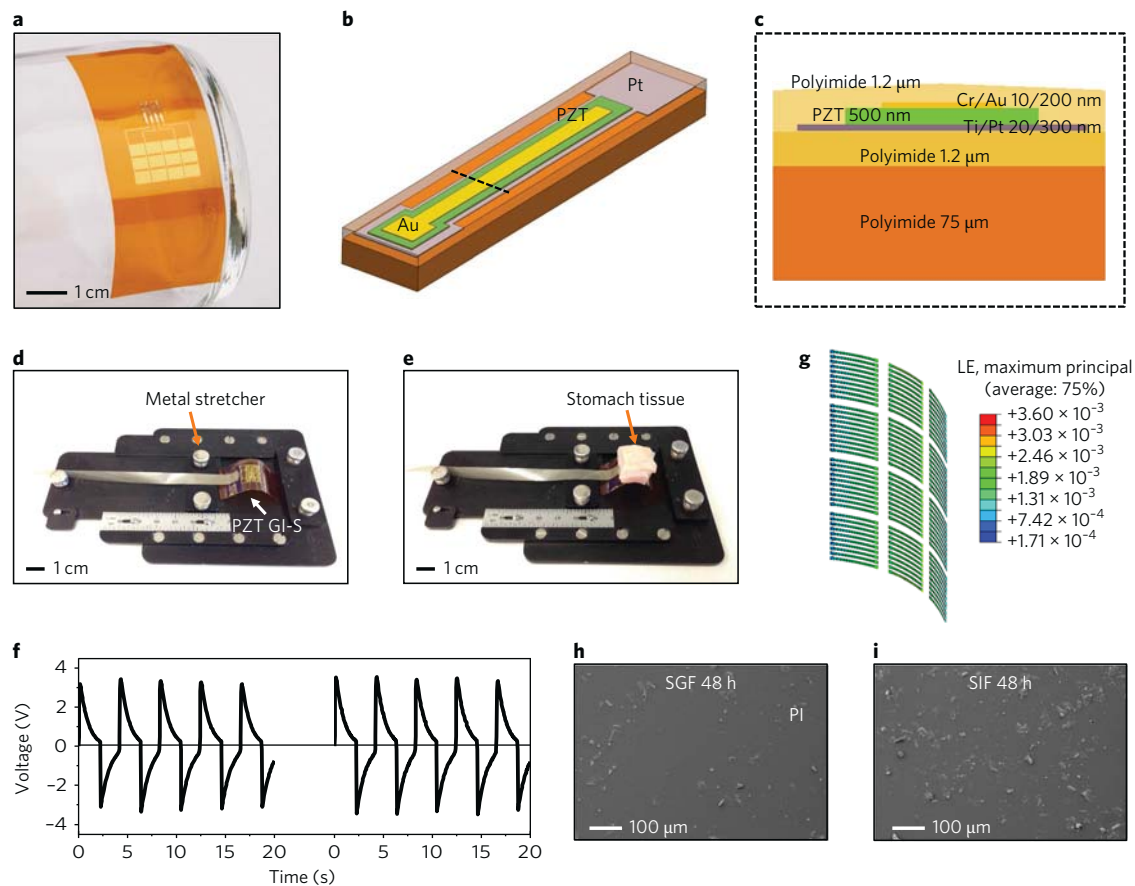


Fig. 1 | PZT GI-S. **a**, Photograph of a PZT GI-S on a glass cylinder. **b**, Schematic illustration of an individual PZT ribbon in **b** at the black dashed line. **c**, Cross-sectional view of the PZT ribbon in **b** at the black dashed line. **d**, Photograph of a bent PZT GI-S. **e**, Photograph of a PZT GI-S with stomach tissue tested via a custom-made metal stretcher. **f**, Corresponding voltage output over time from repeated (10,000) bending cycles as in **d** and **e**. **g**, Strain distribution in a PZT GI-S ribbon during bending. The maximum principal strain is much less than the failure strain in PZT. LE is the logarithmic strain. **h,i**, SEM images of a PZT GI-S after 48 h immersion in simulated gastric fluid (SGF) (**h**) and simulated intestinal fluid (SIF) (**i**).

poly(pyromellitic dianhydride-co-4,4'-oxydianiline) amic acid solution (PI, Sigma–Aldrich) followed by a 10- μm -thick layer of ultraviolet curable epoxy (LOCTITE 5055; Henkel) to provide protection and isolation from the GI environment. Ultraviolet curable epoxy was chosen as the outermost encapsulation layer due to its high bond strength²³. The electrical connections of the module used PTFE hook-up wires (copper conductor, 30 American wire gauge, 0.006 PTFE insulation thickness; Alpha Wire) with a length of 2 m (Supplementary Fig. 1) to attain signal collections via a computer-controllable USB multimeter (U2741A; Keysight) (Supplementary Fig. 2; see Methods). To study the mechanical and electrical stabilities of a PZT GI-S integrated with stomach tissue, we performed mechanical cycling tests with a custom metal stretcher to bend the device without and with a 2 cm \times 2 cm piece of stomach tissue on top, leaving all tissue layers intact (Fig. 1d,e; see Methods). No significant difference in the voltage output from the repeated bending cycles was noted between the cases, as seen in Fig. 1f. The bending results suggest that the PZT GI-S is mechanically and electrically stable over 10,000 cycles. All device layers were modelled as linear elastic materials with properties shown in Table 1. Here, the finite

element simulation revealed that the PZT GI-S buckles to a sinusoidal mode at a very low strain value of $\epsilon = 2.1 \times 10^{-5}$ (Supplementary Fig. 3). Above this threshold, the device compensated for the applied compression via out-of-plane bending, as shown in Fig. 1g, with a maximum strain of $\epsilon = 4 \times 10^{-3}$ in the ribbons. Given that the bending strain was significantly lower than the failure strains of PZT and other materials, the cyclic loading did not lead to fatigue failure of the device^{8,24–26}. Next, we examined the mechanical stability of the PZT GI-S inside the body by immersing the device into simulated gastric fluid and simulated intestinal fluid for 48 h. Scanning electron micrograph (SEM; JEOL 5600LV, 5 kV, 20 spotsize, high voltage, secondary electron imaging (SEI)) images of the module after 48 h of immersion in simulated gastric fluid and simulated intestinal fluid are shown in Fig. 1h,i, respectively. These confirm that the device is mechanically stable over the course of 48 h without any cracks or delamination of the encapsulation layer (Supplementary Fig. 4). We also tested the performance of the PZT GI-S immersed in various solutions with different pH values over 48 h to mimic the change in pH of the gastric fluid depending on several factors such as different GI disease conditions or diet (Supplementary Fig. 5). No major voltage difference was noted before and after repeated (10,000) bending cycles.

Table 1 | Mechanical properties of the layers in the PZT GI-S

Material	Kapton	Ti	Pt	PZT	Au	Cr
Elastic modulus (GPa)	2.5	116	168	63	78	279
Poisson's ratio	0.34	0.32	0.38	0.3	0.44	0.21

Cell culture study and biocompatibility. We investigated the toxicity of the device by performing cell cytotoxicity analyses of GI model cells as recommended by the Food and Drug Administration Guidance of the International Standard (ISO 10993-1 Biological

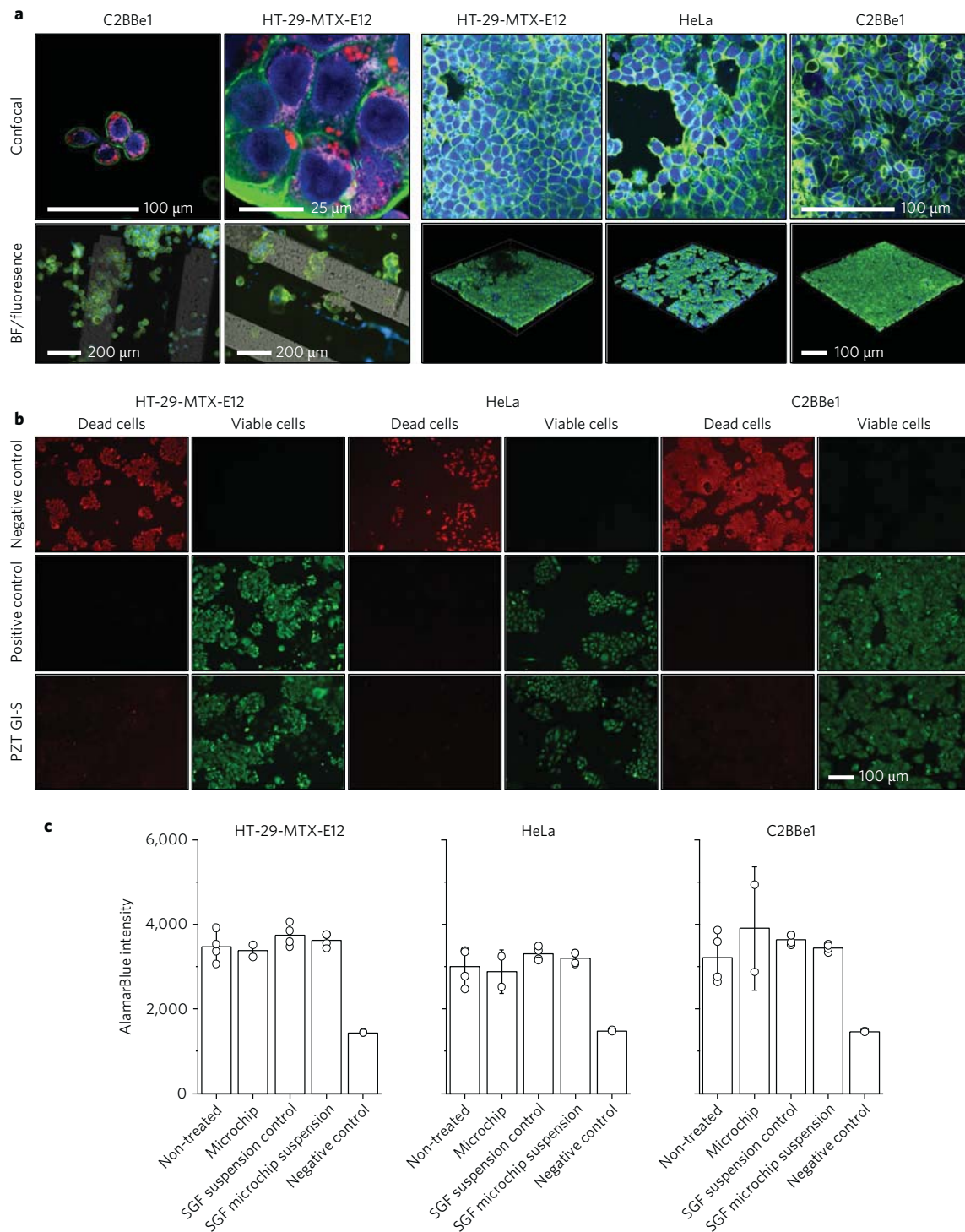


Fig. 2 | Cell culture study and biocompatibility. a, Left: high-resolution confocal microscopy images (top) and fluorescence and bright field (BF) overlap images (bottom) of C2BBe1 and HT-29-MTX-E12 cells grown on the microchip device surface for three days followed by fixation and nucleus (DAPI, blue), F-actin (phalloidin, green) and lysozyme (LysoTracker, red) staining. Right: confocal microscopy images of HT-29-MTX-E12, HeLa and C2BBe1 cells grown on the microchip device surface for three days followed by fixation and nucleus (DAPI, blue) and F-actin (phalloidin, green) staining, including representative confocal sections and a 3D reconstruction of the confocal stack. **b**, Live/dead cytotoxicity analysis of HT-29-MTX-E12, HeLa and C2BBe1 cells incubated with neutralized simulated gastric fluid for three days. The gastric fluid was used as a medium to incubate the microchip devices for three days at 37 °C before neutralization and addition to the cells. Cells treated with 70% ethanol were used as a negative control and cells treated with neutralized gastric fluid that had not been in contact with the microchips were used as a positive control. Green indicates viable cells and red indicates dead cells. **c**, AlamarBlue intensity of HT-29-MTX-E12, HeLa and C2BBe1 cells incubated with neutralized simulated gastric fluid (SGF) for three days (SGF microchip suspension) or the microchip itself (microchip). Cells treated with 70% ethanol were used as negative control and cells treated with neutralized gastric fluid that had not been in contact with microchips (SGF suspension control) or non-treated cells (non-treated) were used as positive controls. The error bars show the standard deviation, with centre values as the mean.

Evaluation of Medical Devices). GI model cells co-incubated with the PZT GI-S or exposed to the released compounds of the device in simulated gastric fluid did not display cytotoxicity as assessed by measuring the cell metabolic activity as well as the plasma membrane integrity (Fig. 2a,b). Through these images, we confirmed by fluorescence and bright field microscopy overlap that the cells were able to adhere to all the different materials of the microfabricated sensor. Furthermore, high-resolution microscopic analysis of GI model cells cultured on the surface of the PZT GI-S revealed cell adhesion and spreading on the device surface. Thus, the collective results support the potential for GI tissue to grow around the device when implanted in the tissue (Fig. 2c). The biocompatibility analysis, however, did not include potential immunogenic reactions that could be triggered by the device, which would need to be investigated in an animal model in subsequent studies.

In vitro assessment of electrical performance. We further confirmed the device functionality by performing in vitro experimental evaluations with a transparent balloon connected to a flow inlet, a pressure gauge and a flow outlet to mimic the stomach (Fig. 3a,b). The system was constructed with ½ inch polyvinyl chloride (PVC) tubing along with the corresponding components and connectors. Unidirectional flow was achieved by using a one-way check valve placed directly after the inlet. All of the connections in the system were made impermeable with either pipe cement or sealant tape. The internal pressure readings were displayed using an SSI Technologies pressure gauge with an operating range of 0–5 psi (see Methods). The in vitro evaluations included two cases: (1) the PZT GI-S free-floating inside the balloon and (2) the PZT GI-S affixed to the inner wall of the balloon with a thin layer (~10 µm) of Loctite Super Glue. In both cases, the PZT GI-S was electrically connected to a USB multimeter to collect voltage outputs. Unless otherwise noted, all of the experiments were conducted with the PI substrate of GI-S in contact with the target substrate. To simulate fluid ingestion into the stomach, a total volume of 200 ml water at room temperature in 50 ml increments was infused into the balloon using a syringe. The rates of water infusion in the in vitro and ex vivo experiments were around 5 ml s⁻¹ and 2.5 ml s⁻¹, respectively, and the duration of the pauses between each 50 ml step of water insertion was 2 s. The resulting effects on a balloon containing a PZT GI-S before and after water infusion can be seen in Fig. 3c,d, respectively. The corresponding voltage outputs from both cases are shown in Fig. 3e,f, respectively. Representative voltage outputs for the floating (Fig. 3g) and glued (Fig. 3h) PZT GI-S showed a steady increase as the pressure built up. The associated average pressure values during water infusion followed a similar trend (Fig. 3i,j). The voltage output due to 200 ml water infusion (four individual trials) yielded four consecutive peaks as the water was infused in 50 ml increments into the balloon (Fig. 3g,h). The initial voltage output (that is, baseline) of a PZT GI-S yielded a constant line, which was expected given that PZT GI-S does not experience any pressure variations (Supplementary Fig. 6). We observed the baseline voltage due to external forces, such as gravity and atmospheric pressure, which were experienced by the devices²¹. We also noted that there was a slight curve difference between the floating and glued balloons. The PZT GI-S in the glued balloon yielded a higher voltage output than the floating one due to the higher effective in-plane strain. When the PZT GI-S floats freely inside the balloon it undergoes large deformations and out-of-plane bending by water infusion. The induced deformations and strains generate a significant voltage output in the PZT ribbons compared with the baseline voltage (see Fig. 3e and Supplementary Fig. 6a). When the device is glued to the balloon wall, its motion is constrained to the in-plane deformations induced by the balloon expansion. Additionally, given that the latex material is significantly softer than the device and the glue, the balloon's expansion mainly occurs in the latex section, not on the device section. The voltage output generated by water infusion when the device was glued

was not significant compared with the baseline voltage (see Fig. 3f and Supplementary Fig. 6b). In ex vivo experiments, the PZT GI-S was in contact with stomach tissue, which is mechanically much softer than the device materials, and behaviour similar to that of the glued PZT GI-S was observed.

ABAQUS/Standard for finite element modelling. Next, we modelled the behaviour of the PZT GI-S device glued to the balloon wall using the finite element method (ABAQUS/Standard; Simulia) to approximate the electrical output as a function of key design parameters, materials properties and applied contractions. The model was made of 120 separated ribbons of five different layers (20 nm Ti, 300 nm Pt, 500 nm PZT, 10 nm Cr and 200 nm Au). All ribbons were mounted on a 75 µm Kapton layer while Kapton was tied to a spherical balloon. All layers were modelled as linear elastic except the balloon, which was modelled as a neo-Hookean hyperelastic, and the PZT ribbons, which were modelled using a built-in piezoelectric material model in ABAQUS (see Methods). Series and parallel electric connections between the PZT ribbons were modelled by constraining the electric potentials between the surfaces of the PZT layers using Tie constraint in ABAQUS. The other mechanical properties of the device were taken from a previous study⁸ (see Methods for more details). The infusion process of the balloon was modelled using the Cavity and Fluid Filling options in ABAQUS/Standard. A total of 200 ml of water was added to the balloon in four steps as shown in Supplementary Fig. 7. Cross-sections of the PZT GI-S device and balloon are shown in Fig. 3k before and after the water infusion. As shown in Fig. 3l, the strain distribution in the ribbon was less than 0.01, which is reported as the failure strain for thin-film PZT ribbons^{20,21}. The PZT GI-S device was modelled in an open circuit in finite element analysis (the electric circuit cannot be modelled in ABAQUS). As shown in Fig. 3m, the maximum electric potential generated by the device was less than 40 mV. We should note that since the finite element model did not consider the electric circuit, the electric potential did not dissipate over time. To model the device in an electric circuit, we developed an approximate analytical model of the PZT patch glued to the balloon (see Methods). As shown in Fig. 3n, the electric potential generated by the device showed four peaks corresponding to the four steps of water infusion. Moreover, given that the change in internal pressure generated in the balloon decreased with each step (Fig. 3i,j,o), the mechanical input to the PZT ribbon and the electric potential generated decreased in the successive steps, as can be seen in Fig. 3n.

Ex vivo assessment of electrical performance. We tested the device performance in the above in vitro setup by substituting a freshly explanted swine stomach for the balloon to mimic the in vivo environment (Supplementary Fig. 8). Here, a swine stomach was procured from a local slaughterhouse 20 min after euthanization (see Methods). After dissection and emptying, the stomach was attached at the level of the gastro-oesophageal junction to the experimental setup. The stomach was ligated at the level of the duodenal bulb to prevent leakage of fluids. Figure 3p,q shows the ex vivo stomach before and after the infusion of 200 ml of water, respectively. The corresponding voltage output is shown in Fig. 3r. The representative graph presents a similar trend as was seen in the in vitro experiments (Fig. 3s,t). The collective results confirm that water infusion in general increases the pressure buildup inside the stomach until a maximum is reached. Thus, the created in-plane strain within the piezoelectric layer of the PZT GI-S, due to the GI pressure, was transformed as a voltage output. Given that latex has an elastic modulus of 1.5 MPa and the measured unstretched volume of a latex balloon was 50 ml, consistent initial pressure readings with instilled water volumes were observed. In contrast, the swine stomach had a resting unstretched volume of approximately 1–2 l and the measured swine gastric mucosa yielded an elastic modulus

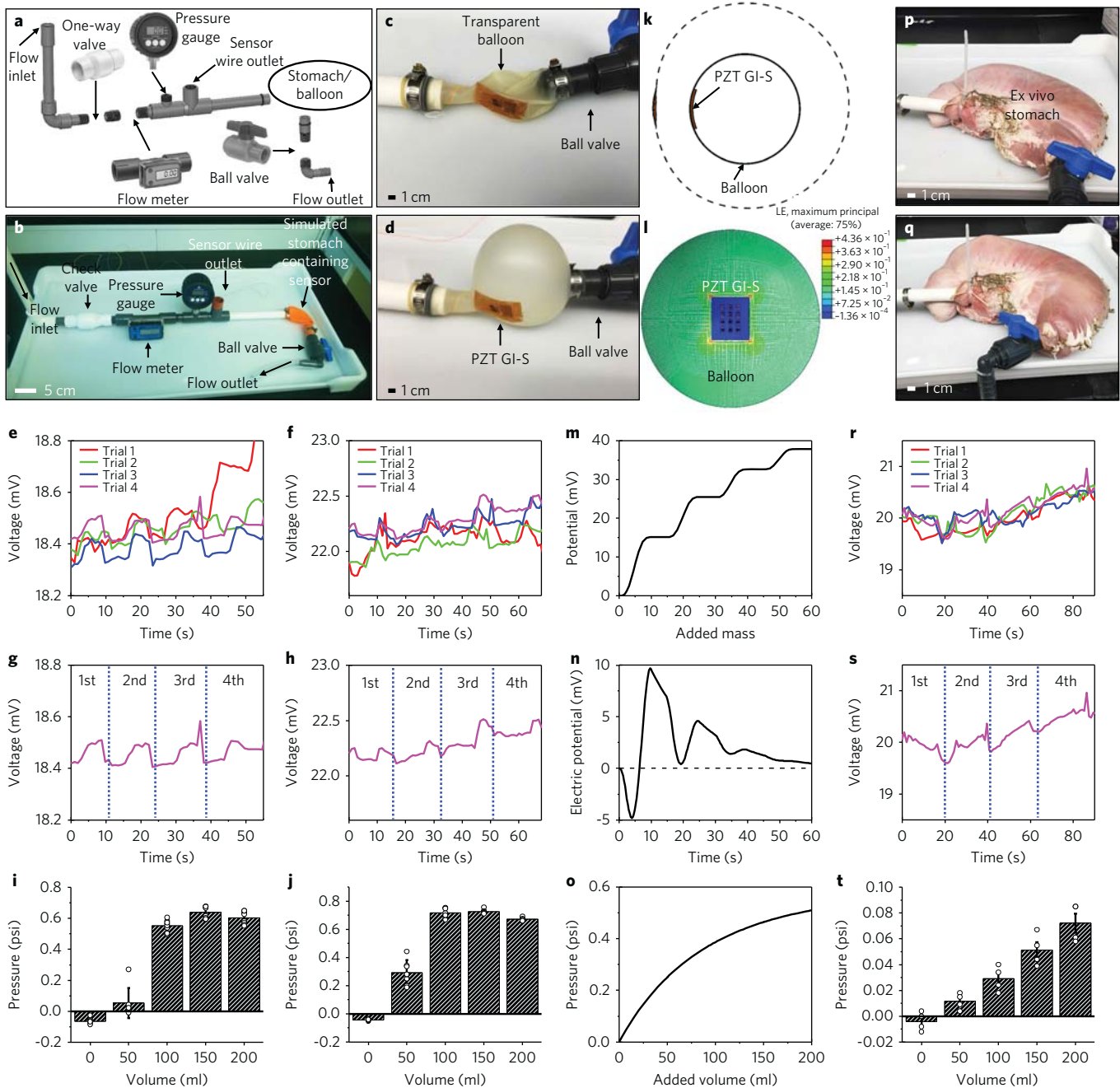


Fig. 3 | In vitro experimental characterization. **a, b**, In vitro setup to simulate stomach behaviour shown as a schematic illustration (**a**) and photograph (**b**). **c, d**, Stomach simulation setup showing a transparent balloon before (**c**) and after (**d**) 200 ml water infusion. **e, f**, Voltage-versus-time graphs for a floating (**e**) and glued (**f**) PZT GI-S in a balloon with 200 ml water infusion (50 ml increments). **g, h**, Representative voltage-output-versus-time graphs for every 50 ml water infusion for a floating (**g**) and glued (**h**) PZT GI-S in a balloon. **i, j**, Graphs of average pressure variation during the water infusion in **e** and **f** for a floating (**i**) and glued (**j**) PZT GI-S in a balloon. **k**, Finite element model of a PZT GI-S device attached to a hyperelastic spherical balloon. Both undeformed (black solid line) and inflated (black dashed line) stages are shown. The mechanical deformations of the balloon and PZT GI-S are magnified three times. **l**, Strain distribution in a PZT GI-S generated by infusing the balloon with 200 ml incompressible fluid. LE is the logarithmic strain. **m**, Electric potential generated with a PZT GI-S obtained from the finite element model in an open circuit. **n**, Electric potential generated by the device obtained from the approximate analytical model. **o**, Pressure generated in the balloon versus the water infused. **p, q**, Photographs of an ex vivo stomach integrated with the in vitro setup before (**p**) and after (**q**) 200 ml water infusion. **r**, Voltage-versus-time graph for a PZT GI-S in an ex vivo stomach with 200 ml water infusion (50 ml increments). **s**, Representative voltage-output-versus-time graph for every 50 ml water infusion for a PZT GI-S in an ex vivo stomach. **t**, Graph of the average pressure variation during the water infusion shown in **r** and **s**. The error bars in **i, j** and **t** show the standard deviation, with centre values as the mean.

of 0.7 MPa ± 0.1 (Supplementary Fig. 9). This large difference in volume between the balloon and stomach, while still infusing the same amount of water, allowed only the balloon model to reach a maximum internal pressure during testing. The increasing nature

of the relationship between the stomach's volume and pressure is, therefore, comparable to only the initial segment of the curve describing the balloon's relationship between volume and internal pressure, before the maximum is reached (see Methods). With the

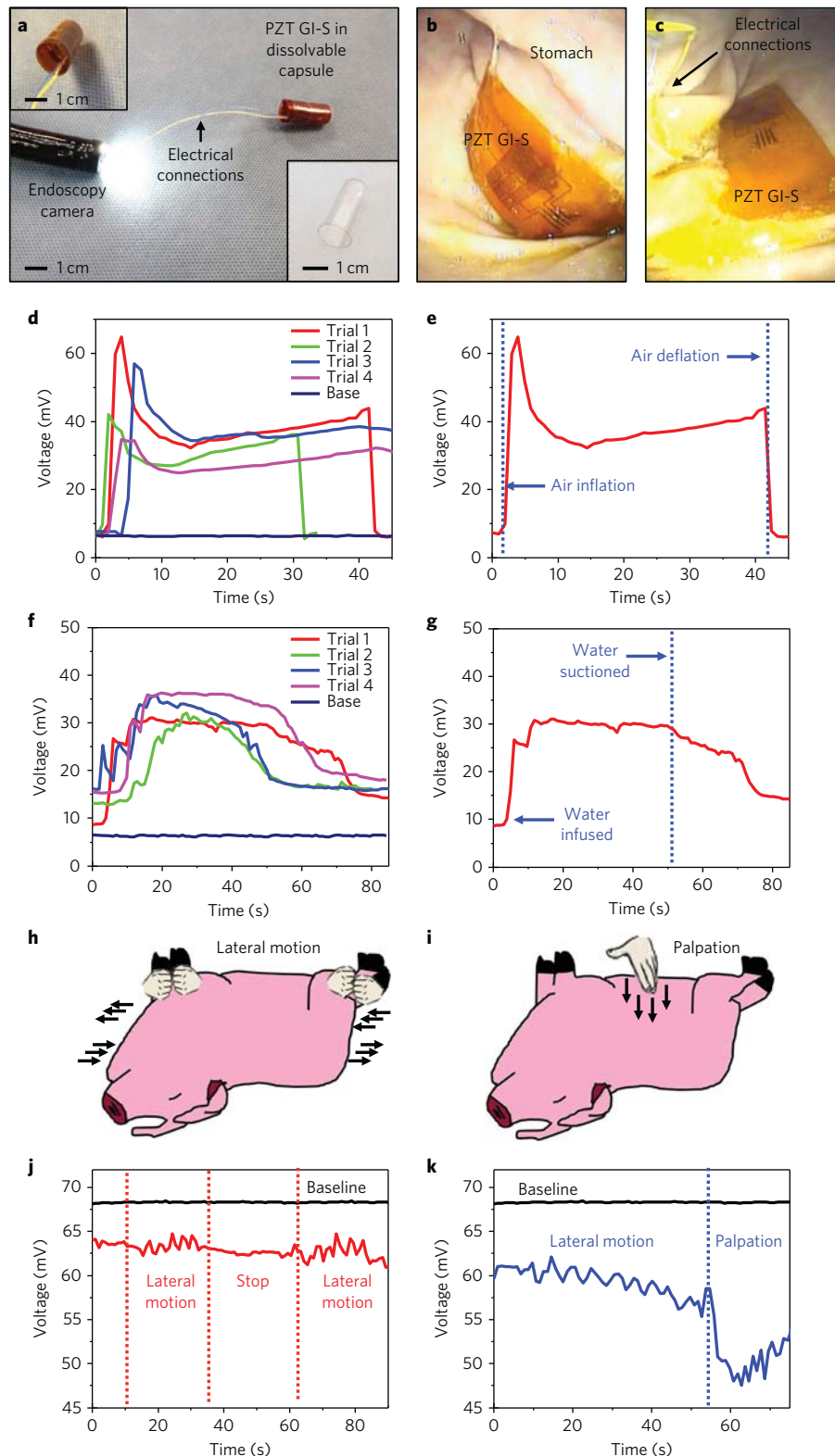


Fig. 4 | In vivo evaluation in Yorkshire swine model. **a**, Photograph of the PZT GI-S setup before insertion into a swine stomach. The top left inset shows the rolled PZT GI-S inside a dissolvable capsule (bottom right inset). **b, c**, Photographs of the PZT GI-S on the wall of the stomach during inflation (**b**) and deflation (**c**). **d**, Corresponding voltage output graphs from the inflation and deflation shown in **b** and **c**. **e**, Representative voltage-output-versus-time graph of a cycle of inflation and deflation. **f**, Graph of voltage versus time for the PZT GI-S in the swine stomach during 200 ml water infusion in 50 ml increments. **g**, Representative voltage output versus time for a cycle of water infusion and suction. **h**, Illustration of lateral motion on the swine to mimic animal walking movements. **i**, Illustration of abdominal palpation on the stomach of the swine to mimic the stomach movement. **j**, Corresponding output voltage graph generated from the lateral motion-resting cycles in **h** with an absolute displacement value of 10 cm. **k**, Associated output voltage graph obtained from the lateral motion-palpation cycle in **i**.

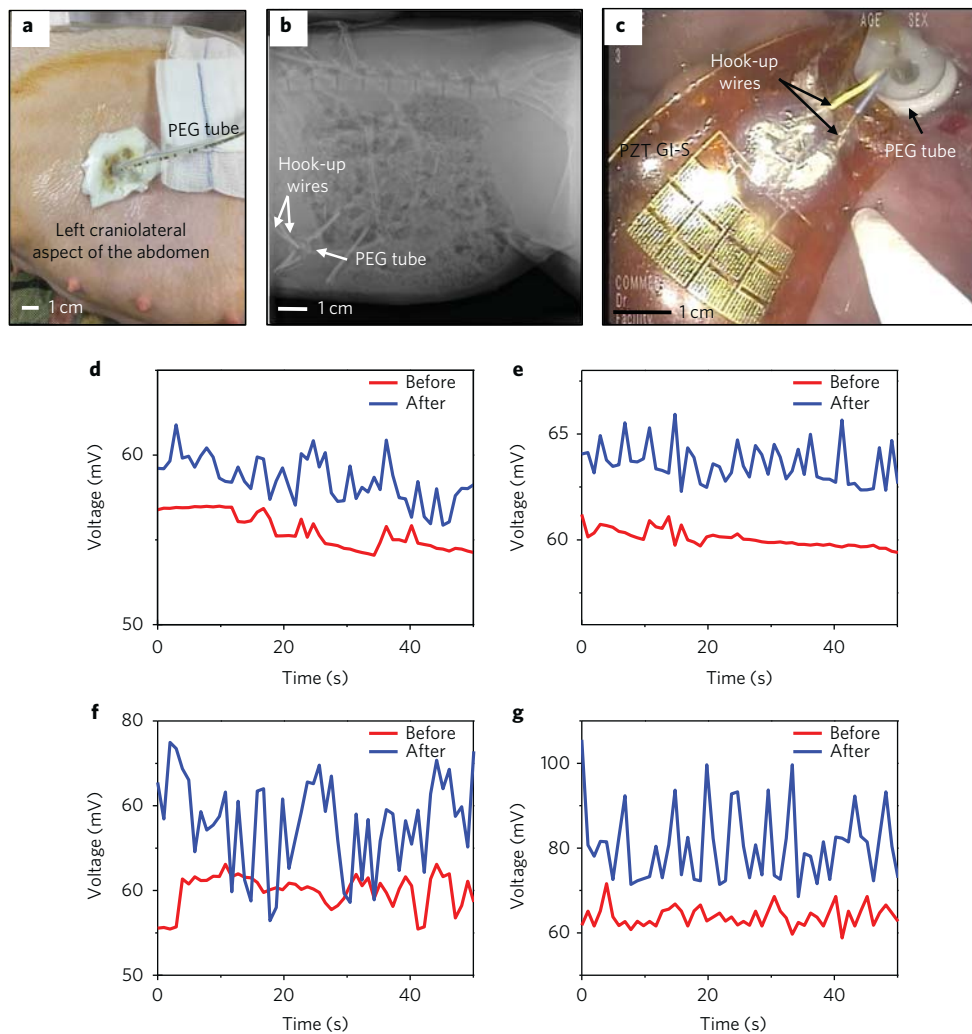


Fig. 5 | In vivo evaluation in a Yorkshire swine model. **a**, Photograph of a PZT GI-S placed on the left craniolateral aspect of the swine abdomen via 20 French percutaneous endoscopic gastrostomy (PEG) tube. Using endoscopic guidance and an overtube, the PZT GI-S attached to electronic connection wires was passed into the stomach and the wires were externalized through the PEG tube. **b**, X-ray image of PZT GI-S in the stomach of the swine taken after three days. **c**, Photograph of the PZT GI-S with PEG tube inside the stomach. **d–e**, Voltage output graphs for morning (**d** and **f**) and afternoon (**e** and **g**) trials from before and after milk ingestion on day 1 (**d** and **e**) and day 2 (**f** and **g**).

latex balloons being about twice as stiff and having a significantly smaller initial volume, higher pressures were anticipated compared with the ex vivo stomach. This was supported by the observation that pressure values from the stomach were an order of magnitude below those of the latex balloon. Even with the disparity in pressure readings of in vitro and ex vivo experiments, the voltage outputs from both arrangements exhibited comparable values and similar positive trends with respect to the volume of water infused.

In vivo evaluation in a Yorkshire swine model. We further confirmed the functionality of the PZT GI-S in a large animal model. Two Yorkshire swine of around 45 kg in weight were briefly sedated, intubated and maintained on isoflurane (see Methods). To place the PZT GI-S in the gastric cavity endoscopically, we folded the flexible device in a dissolvable gelatin capsule (Fig. 4a). It took around 5 min²⁷ for the gelatin capsule to dissolve, around 10 s for it to unfold and around 5 s for it to settle on the stomach lining (Supplementary Fig. 10). A PZT GI-S with a 75- μm -thick polyimide substrate and lateral dimensions of 2.5 cm (length) \times 2 cm (width) showed an average adhesion force of 0.064 N (see Methods). Detachment of the PZT GI-S from the stomach lining during the application with

an average adhesion force of 0.064 N was unlikely. Since the GI-S compensated for the applied compression via out-of-plane bending with a maximum strain of $\varepsilon = 4 \times 10^{-3}$ in the ribbons (Fig. 1g), folding the device did not induce any mechanical or electrical problems. As the capsule dissolved in the GI fluid, the PZT GI-S unfolded naturally (Supplementary Fig. 10a) and settled intimately onto the stomach lining (Supplementary Fig. 10b). To mimic gastric expansion secondary to ingestion, serial air and water instillments were performed and data were collected during these treatments (Fig. 4b,c). The inflation and deflation trials (four individual trials) are shown in Fig. 4d. In the in vivo experiments, the baseline voltage (Supplementary Fig. 6) was also observed, because the pressure values were influenced by not only external forces, but also internal forces, such as those from the muscles and fluids^{28–30}. A representative voltage-output-versus-time graph of a cycle of air inflation and deflation is shown in Fig. 4e. When air was introduced in the stomach, the PZT GI-S experienced a sudden pressure change that resulted in a significant voltage increase from around 10 mV to 60 mV. Over the course of 40 s of inflation, the inner pressure stabilized and resulted in a plateau voltage curve, whereas a substantial decrease in voltage from around 40 mV to the base state occurred

as the air was released. Here, the potential to sense changes associated with air ingestion suggests the capacity to guide evaluation and treatment in cases of aerophagia or significant small intestine bacterial overgrowth, as well as in disaccharidase deficiencies where excess gas can manifest in pain^{31,32}.

A second experiment was conducted in which 200 ml water was instilled in 50 ml increments (four separate trials) into the stomach, and the voltage output from the PZT GI-S was recorded (Fig. 4f). Having observed the dynamic changes associated with air insufflation and deflation (Fig. 4d,e), the changes in the gastric content volume were evaluated for water. The representative voltage output versus time of the cycle of water infusion and suction is indicated in Fig. 4g. The 200 ml water intake into the stomach resulted in an increase in the voltage output from around 8 mV to 30 mV incrementally with respect to a repetitive 50 ml water infusion. As in the deflation case, a substantial decrease in voltage from around 30 mV to around 15 mV was observed due to the water outlet. The initial voltage output (baseline) of a PZT GI-S yielded a constant line, as in the *in vivo* and *ex vivo* tests, because there was no pressure variation. In this case, the voltage did not return to the initial state because of the remaining water inside the stomach. We note that the capacity to sense fluids raises the potential of sensing general foodstuffs, which could add a new mode of evaluation of patients suffering from obesity.

Next, we simulated walking animal activity that could potentially be used to harvest mechanical energy from GI motility by applying lateral motion and abdominal palpations directly on the stomach of a sedated animal (Fig. 4h,i). The output voltage recorded during abdominal palpation demonstrates the ability to sense GI motility due to food ingestion and the potential functionality to simultaneously generate electrical power. The associated output voltage during the lateral motion and resting cycles and abdominal palpation on the stomach of the swine to simulate the stomach movement are summarized in Fig. 4j,k. Figure 4j shows a periodic voltage output, which is consistent with the lateral motion–resting cycle. The voltage output was, however, slightly (~10 mV) low when abdominal palpation was applied, as shown in Fig. 4k. Additional trials are shown in Supplementary Fig. 11. Future work should focus on incorporating an electromagnetic field-based wireless system for prolonged powering and communication³³ with the PZT GI-S.

In vivo ingestion motility evaluation in a Yorkshire swine model.

To validate the *in vivo* capacity for motility monitoring, we conducted experiments in awake and ambulating Yorkshire swine. Specifically, the PZT GI-S was placed in the gastric cavity and awake ambulatory communication with it was enabled through externalization of the connectors via a percutaneous gastrostomy (PEG) tube (Fig. 5a). The positioning was confirmed endoscopically and radiographically (Fig. 5b,c). The animal recovered well from PEG placement, and repeated measurements in an awake and ambulating swine were performed twice a day 24 and 48 h following placement of the device. The voltage outputs were collected while the animal ambulated and during milk ingestion. The corresponding voltage output graphs for morning (Fig. 5d,f) and afternoon (Fig. 5e,g) trials of before and after milk ingestion during day 1 and day 2 demonstrated consistent voltage increases during ingestion. Not only did the device demonstrate the capacity to perform in an awake and ambulating large animal, but—reassuringly—it remained fully functional following exposure to the gastric environment for 48 h. Together, the reported results provide evidence that the PZT GI-S exhibits mechanical and electrical robustness that enables stable operation inside the gastric cavity while providing a consistent and relevant evaluation of the motility states of the stomach. Additionally, these preliminary experimental results support the possibility of modifying this flexible device for the purposes of energy harvesting, in the form of a self-powered system that is more compatible with ingestion.

Discussion

The concepts in materials and characterization methods introduced here provide new routes to monitor vital signs and associated mechanical deformations of the gastric cavity. This in turn could aid in the diagnosis and treatment of motility disorders and in the monitoring of ingestion for applications in the treatment and evaluation of obesity. The small dimensions and flexible nature of this device could reduce the likelihood of GI tissue damage, and thereby maximize its broad applicability. Furthermore, the device flexibility not only allows for robust contact with soft tissues inside the stomach during gastric motion, but also enables compact packaging of the device within dissolvable capsules, facilitating oral delivery. *In vivo* pre-clinical measurements, along with those on *ex vivo* organs integrated with an *in vitro* setup, show consistent performance in the GI tract or cavity, and corroborate its practical functionality. Future embodiments might incorporate a wireless network, bioresorbable material components, a further miniaturized device design with multilayer configurations to realize capabilities in transient and remotely controlled GI sensors, and mechanical energy harvesters.

Methods

Fabrication of PZT GI-S and electrical connection. The fabrication steps of a PZT GI-S were described in a recent study by Dagdeviren et al.^{8,10}. The PZT GI-S module was further encapsulated with a 1.2- μm -thick layer of polyimide and a 10- μm -thick layer of ultraviolet curable epoxy (LOCTITE 5055; Henkel). The electrical connection between the module and the computer-controllable USB multimeter was created via PTFE hook-up wires (Cu conductor, 30 American wire gauge, 0.006 PTFE insulation thickness; Alpha Wire). The output metal trace of the PZT GI-S module and hook-up wire was soldered with lead-free solder (Sn96 Ag3.0 Cu0.5; Kester) using a digital soldering station power (WD1; Weller). Four identical PZT GI-Ss were used to perform the demonstrations in Figs. 3 and 4, with a single trial using each of the individual devices.

Study of pH. Aliquots (500 ml) of phosphate-buffered saline (PBS; Thermo Fisher Scientific), pH 7.4 were adjusted to pH values of 2, 3.5 and 5 via the dropwise addition of hydrochloric acid ACS reagent, 37% (catalogue number 320331 and CAS 7647-01-0; Sigma-Aldrich). The pH values were measured using an InLab Expert Pro pH electrode (Mettler Toledo) combined with a pH/mV bench meter (Mettler Toledo).

In vitro test setup. A 30.48 cm length of standard 1/2 inch unthreaded PVC tubing was attached to 1/2 inch PVC coupling at the top and 90° PVC elbow at the bottom. Into the other end of the elbow, a 1/2 inch PVC thread-one-end pipe nipple was connected. An NSF-certified PVC check valve was threaded onto PVC tubing to guarantee unidirectional flow. Threaded into the outflow end of the valve was a fully threaded 1/2 inch PVC pipe nipple. This was connected to a GPI TM Series water meter/totalizer that had an accuracy of $\pm 3\%$ full scale (FS) and the ability to operate in a temperature range from 0° to 60°C. Another 1/2 inch PVC thread-one-end pipe nipple was used to connect the meter to a PVC tee fitting with a steel threaded inline reducer. Threaded into the top of the tee was an SSI Technologies MG1-5-A-9V-R pressure gauge, which had an operating range of 0–5 PSI and –10° to 60°C with an accuracy of $\pm 1\%$ FS. Into the first tee was the male end of a PVC tee with two female ends. An 8 inch length of standard 1/2 inch unthreaded PVC tubing was inserted into one female end. In the other, a rubber septum stopper from Chemglass was placed with a small hole drilled into it for the wires of the device to exit the system. The wires were glued into place and made water-tight using Loctite Super Glue Professional Liquid.

A clear 12 inch latex balloon was used as a stand-in for the stomach. In the experiments with the device fixed to the balloon, Loctite Super Glue Professional Liquid was used to adhere the device to the inside of the balloon. The mouth of the balloon was slid onto the end of the 8 inch PVC pipe over top of two rubber 1/16 inch O-rings. A worm drive steel hose clamp was used to secure the balloon in place. A small hole was cut in the top of the balloon so it could be secured to the unthreaded end of a 1/2 inch PVC thread-one-end pipe nipple in the same fashion as previously mentioned. The nipple was threaded into a low-pressure PVC ball valve that could be opened to release fluids from the system. Fluids were administered to the test system at the top of the one-foot length of PVC using a 60 ml oral medication syringe (Monojet). This was pushed through a rubber septum stopper (Chemglass) with a small hole drilled into it to form a seal. All unthreaded connections in the test system were sealed using plastic pipe cement for PVC. All threaded connections were sealed with commercial-grade pipe thread sealant tape.

Pressure change in the balloon. It is a known fact that natural rubber does not deform according to Hooke's law, thus creating a non-linear relationship between a latex balloon's volume and internal pressure. Merritt and Weinhaus²⁹ derived an equation to relate the internal pressure of a balloon to its radius. They generated a theoretical pressure curve, which increases rapidly to a pronounced peak and then gradually drops to zero as the radius approaches infinity²⁹. Such a formula can be transformed and used to predict the radius at the maximum internal pressure:

$$r_p = 1.38r_0 \quad (1)$$

where r_p is the radius at maximum internal pressure and r_0 is the uninflated radius. Assuming the balloon is a sphere and the initial volume of the balloon is 50 ml, the initial radius can be calculated using the formula

$$V = \frac{4}{3}\pi r^3 \quad (2)$$

where V is the volume and r is the radius. This yields an initial radius of 2.29 cm, which is used as r_0 in equation (1) to calculate r_p (3.16 cm). The r_p is then used as the radius in equation (2) to determine the volume of the balloon at which the internal pressure is at a maximum (~132 cm³ or 132 ml). Considering the pressure readings from the balloon in Fig. 3i,j, it is reasonable to assume that the maximum pressure in the balloon occurred between the volume intervals of 100 and 150 ml, which correlates with the predicted value. Therefore, the collected balloon pressure readings appear as expected and follow the trend of Merritt and Weinhaus' theoretical pressure curve²⁹.

Ex vivo tissue preparation. All procedures were conducted in accordance with protocols approved by the Massachusetts Institute of Technology (MIT) Committee on Animal Care. A swine oesophagus, stomach, and a portion of the small intestine after the duodenum were harvested twenty minutes after euthanization from a local slaughterhouse. The contents were held in a chilled container at approximately 4°C during its transport. The stomach was then moved to a sterile hood and a dissection was performed. The oesophagus was removed from the stomach with medical scissors along the gastro-oesophageal junction. The gastric contents were emptied using a 60 ml Monojet oral medication syringe and water in order to remove any particulate that had adhered to the mucosal layer, which could potentially interfere with adhesion of the device and the experimental readings. The small intestinal tract was then removed after the duodenum by using medical scissors. At no point were any other incisions made in the stomach tissue, ensuring structural and fluidic integrity. After dissection, the stomach was attached at the level of the gastro-oesophageal junction to the experimental setup. The stomach was ligated at the level of the duodenal bulb to prevent leakage of fluids during the experiments.

On another occasion, a similar dissection occurred including the removal of the oesophagus at the gastro-oesophageal junction and the small intestine after the duodenum. In this instance, the stomach tissue was extracted in 2 cm × 2 cm sections (Fig. 1e) leaving all tissue layers intact to test adhesion of the device to the mucosal layer. The extracted tissue was placed in a solution of Gibco 1x Dulbecco's phosphate-buffered saline (DPBS) and stored at 4°C until testing occurred.

Stomach tissue harvesting. All procedures were conducted in accordance with protocols approved by the MIT Committee on Animal Care. A swine GI tract was collected from Lemay & Sons Beef LLC in Goffstown, NH, USA. The tissue was transported in a cooler and when it arrived at the MIT, it placed on ice and transferred in a laminar flow hood for dissection. The stomach was dissected from the gastro-oesophageal junction and duodenum to separate the stomach from the GI tract. An incision was made in the anterior wall where a section of stomach was removed (epithelial and muscle layers intact). From there, the epithelial layer was detached from the muscle layer by carefully cutting the loose connective tissue using scissors. The new sections were cut into approximately 23.5 mm × 60 mm pieces.

Stomach tissue characterization. The tension of the newly sectioned samples was tested in on an Instron 5943, which was running Bluehill 3 software. Specially designed grip faces were fabricated to test the tissue samples in screw-action grips, to avoid tissue slippage. The samples were placed between the grip faces and clamped down leaving a gauge length of 17.5 mm for testing. The test ran at an extension rate of 0.05 mm s⁻¹. The samples were pulled until failure. The entirety of this experiment, from harvesting to tissue failure, was approximately 5–6 h. The data from the tensile testing of the sections of the epithelial layer were used for analysis.

Raw data were taken from the Instron and plotted to show stress as a function of strain. Because of tissue's poroelastic nature, only the initial phase of the stress-strain curve could be used to determine elastic moduli. Therefore, the data were truncated to a strain range of 0.4 to 0.45 to capture a linear portion within this initial phase. The elastic modulus was determined for each tissue sample individually by calculating the ratio of the increments of tensile stress to the increments of strain. These values were used to calculate the average and standard

deviation of the elastic modulus of swine epithelial tissue. Supplementary Fig. 9 shows the truncated stress-strain curve of the swine gastric mucosa samples.

Adhesion test. The adhesion strength was measured using a digital force meter (Mark-10; USA), using the following procedures from ref. ³⁴. The stomach was secured and the device substrate was connected to a force meter. The PZT GI-S was peeled away at a maximum speed of 1,000 mm min⁻¹ in an upward direction, parallel to the width of the device, at room temperature. The maximum value of the force during this process defined the adhesion force. A PZT GI-S with a 75-µm-thick polyimide substrate and lateral dimensions of 2.5 cm (length) × 2 cm (width) showed an average adhesion force of 0.064 N. The detachment of the PZT GI-S from the stomach lining during the application with an average adhesion force of 0.064 N was unlikely. PZT GI-S had intimate integration on the stomach lining (Supplementary Fig. 10b).

SEM. The morphology of the PZT GI-S module surface was observed using the JEOL 5600LV SEM located at the MIT Whitehead Institute. Before visualization under SEM, all samples were sputter-coated with carbon using a Hummer 6.2 Sputter Coater. Samples were cut to be under 0.5 cm² in area and fixed to the aluminium stubs using double-sided adhesive carbon conductive tape.

Cell culture study. HT-29-MTX-E12 cells were purchased from the European Collection of Authenticated Cell Cultures operated by Public Health England. HeLa cells were purchased from the American Type Culture Collection. Both were cultured in Dulbecco's modified Eagle's medium high glucose pyruvate (11995-065), 10% foetal bovine serum (heat inactivated) (catalogue number 10082-147; Life Technologies), 1% Gibco MEM Non-Essential Amino Acid Solution (catalogue number 11140-050; Life Technologies) and 1% Pen/Strep (catalogue number 15140122; Life Technologies) under standard cell culture conditions (37°C and 5% CO₂). C2BBE1 cells were purchased from the American Type Culture Collection and cultured in Dulbecco's modified Eagle's medium high glucose pyruvate (11995-065), 10% foetal bovine serum (heat inactivated) (catalogue number 10082-147; Life Technologies), human Gibco Insulin-Transferrin-Selenium (ITS-G) 100x (catalogue number 41400-045; Life Technologies) and 1% Pen/Strep (catalogue number 15140122; Life Technologies) under standard cell culture conditions (37°C and 5% CO₂). For the experiments, cells were detached using 0.25% (v/v) Trypsin-EDTA solution (Invitrogen). All cells tested negative for mycoplasma contamination.

Immunohistochemical staining. Cell samples were fixed with 4% (v/v) formalin in PBS for 30 min at room temperature, washed with PBS, permeabilized with 0.25% (v/v) Triton-X-100/PBS for 2 min, washed with PBS and then blocked with 4% (w/v) bovine serum albumin in PBS for 1 h. Then, the samples were stained with ActinGreen 488 ReadyProbes Reagent for 40 min followed by 4',6-diamidino-2-phenylindole (DAPI) for 10 min (both purchased from Life Technologies). The samples were washed three times and then mounted on a cover slide using ProLong Diamond Antifade Mountant (Thermo Fisher Scientific).

Microscopical analysis. Light microscopy analysis of the cell samples was conducted using an EVOS FL Imaging System with 10x or 20x air objectives. Fluorescent samples were analysed using a Nikon A1R Ultra-Fast Spectral Scanning Confocal Microscope in a Galvano scanner using a 20x or 10x air objective. The resulting raw images were analysed using NIS-Elements C software (Version 4.20) and ImageJ (Version 1.50i).

Cell viability analysis. Cell cytotoxicity analysis was performed based on the International Standard ISO 10993 (Biological Evaluation of Medical Devices) experimental guidelines. The cytotoxicity of the device in direct contact with cells as well as the cytotoxicity of released compounds in simulated gastric fluid (Sigma, 01651) was tested. Cells were seeded at a density of 20,000 cells cm⁻² in a 48-Well Cell Culture Plate (Corning Costar; Sigma-Aldrich) containing the sterilized device or the sterilized release medium. The release medium consisted of simulated gastric fluid that was incubated with the device for three days at 37°C. Before being used for cytotoxicity analysis, the medium was neutralized using NaOH followed by sterile filtration. Cells were incubated for three days without exchanging the medium. Then, an AlamarBlue Cell Viability assay (catalogue number DAL1100; Life Technologies) and a LIVE/DEAD Viability/Cytotoxicity Kit assay for mammalian cells (catalogue number L3224; Life Technologies) were performed for intact tissue explants according to the manufacturer's protocol using intestinal tissue treated with 70% (v/v) ethanol (ACS reagent, ≥ 99.5%; Sigma-Aldrich) in sterile filtered deionized water for 1 h as a negative control.

In vivo anaesthetized animal study. All procedures were conducted in accordance with protocols approved by the MIT Committee on Animal Care. Randomization of the animals was not performed. Two separate female Yorkshire swines weighing approximately 45–50 kg were used for the in vivo evaluation of the GI-S system. The morning feed was held on the day of the procedure and the animals were sedated with 5 mg kg⁻¹ Telazol (tiletamine/zolazepam), 2 cmg kg⁻¹ xylazine and

0.04 mg kg⁻¹ atropine. To confirm gastric deployment of the PZT GI-S system, an oesophageal overtube (US Endoscopy) was placed in the oesophagus and the gastric cavity was accessed endoscopically. Air was instilled with the aid of a Pentax EPK-I Endoscope Processor and water instilled into the stomach through the access port in the endoscope.

In vivo awake large animal study. All procedures were conducted in accordance with protocols approved by the MIT Committee on Animal Care. A female Yorkshire swine of approximately 50 kg was anaesthetized with tiletamine/zolazepam, xylazine and atropine (4 mg kg⁻¹, 2 mg kg⁻¹ and 0.04 mg kg⁻¹, respectively, via intramuscular administration). The animal was intubated and maintained on 2–3% isoflurane in oxygen. Lidocaine (1%) was administered locally and a 20 French PEG tube (MIC Kit 7160-20; Halyard Health) was placed on the left cranial aspect of the abdomen. Using endoscopic guidance and an overtube, the PZT GI-S attached to the electronic connection wires was passed into the stomach and the electronic connection wires were externalized through the PEG tube. The PEG tube and wires were secured using a bandage. The animal recovered well and recordings were obtained while the animal ambulated and ingested food. The animal was maintained on a liberal diet.

ABAQUS/Standard for finite element modelling. We used ABAQUS/Standard for the finite element modelling of the mechanical behaviour of the PZT GI-S under compression and in interaction with an inflating balloon. Considering the device design, the PZT GI-S was modelled as a multi-layer structure of (1) a 75 μm Kapton layer, (2) a 20 nm layer of Ti, (3) a 300 nm layer of Pt, (4) a 500 nm layer of PZT, (5) a 10 nm layer of Cr and (6) a 200 nm layer of Au (see Supplementary Fig. 12). All layers were modelled as linear elastic materials with the properties shown in Table 1. Moreover, the balloon was modelled as a hyperplastic material with $\mu = 0.5$ MPa and $K = 250$ MPa, where μ and K are the shear and bulk modulus, respectively.

The piezoelectric behaviour of the PZT layer was modelled using the built-in piezoelectric material model in ABAQUS (see ref. ⁸ for values). The overlapping surfaces of different layers were constrained to move with each other using TIE constraints in ABAQUS. Moreover, the series and parallel electric connections were generated by constraining the electric potential between the different surfaces of the PZT layers. The mechanical behaviour of the device was modelled in a Static Step without considering any large deformation (NLGEOM = OFF). The instability of PZT GI-S was modelled using the Buckle Module of ABAQUS. The first buckling mode of the device under compression is shown in Supplementary Fig. 13. The inflation of the balloon was modelled using the Fluid Filling and Fluid Flux options in ABAQUS. The added mass versus time to the balloon is shown in Supplementary Fig. 7. The strain in the structure is illustrated in Supplementary Fig. 13.

To approximate the electric output of PZT GI-S analytically, we found the strain generated inside the device by water infusion. To this end, we note that a single-layer hyperelastic balloon experiences equibiaxial stress as

$$\sigma_\theta = \sigma_\phi = \sigma = \mu \left(\lambda^2 - \frac{1}{\lambda^4} \right) \quad (3)$$

where $\lambda = r/R$ is the principal stretch (R and r are the balloon radius before and after deformation) and μ is the shear modulus of the material^{35,36}. Also, the internal pressure generated by water infusion can be obtained as

$$P = \frac{2\mu H}{R} \left(\frac{1}{\lambda} - \frac{1}{\lambda^7} \right) \quad (4)$$

If a planar piezoelectric patch is glued to the balloon wall, the balloon deformation pattern in the glued area will change. Particularly, if the patch is circular and much stiffer than the balloon material, we can neglect the deformation of the patch. Moreover, we can assume the deformation in the rest of the balloon is not affected by the circular patch and, hence, the balloon remains almost spherical even after deformation. Using these simplifications, equations (3) and (4) are still valid for pressure and stresses in the balloon section while the volume of the balloon can be calculated as

$$V = \frac{\pi r^3}{3} (2 + 2 \cos \gamma + \cos \gamma \sin^2 \gamma) \quad (5)$$

where $\gamma = \rho/r$. Using these formulae we can approximate the stresses in the balloon and then transfer the same stresses to the kapton section and ribbons using the rule of mixture for composite materials³⁷. Having obtained the stresses in the PZT ribbons and assuming linear elasticity, the strain and electric potential in the system was calculated using similar formulas to those suggested in ref. ⁸.

Data availability. The data that support the findings of this study are available within the paper and its Supplementary Information.

Received: 19 March 2017; Accepted: 2 September 2017;
Published online: 10 October 2017

References

- Jacobson, B. & Mackay, R. S. A pH-endoradiosonde. *Lancet* **272**, 1224 (1957).
- Cassilly, D. et al. Gastric emptying of a non-digestible solid: assessment with simultaneous SmartPill pH and pressure capsule, antroduodenal manometry, gastric emptying scintigraphy. *Neurogastroenterol Motil.* **20**, 311–319 (2008).
- Belknap, R. et al. Feasibility of an ingestible sensor-based system for monitoring adherence to tuberculosis therapy. *PLoS ONE* **8**, e53373 (2013).
- Traverso, G. et al. Physiologic status monitoring via the gastrointestinal tract. *PLoS ONE* **10**, e0141666 (2015).
- Iddan, G., Meron, G., Glukhovskiy, A. & Swain, P. Wireless capsule endoscopy. *Nature* **405**, 417 (2000).
- Au-Yeung, K. Y. et al. Early clinical experience with networked system for promoting patient self-management. *Am. J. Manag. Care* **17**, e277–e287 (2011).
- Liao, Z., Gao, R., Xu, C. & Li, Z. S. Indications and detection, completion, and retention rates of small-bowel capsule endoscopy: a systematic review. *Gastrointest. Endosc.* **71**, 280–286 (2010).
- Dagdeviren, C. et al. Conformal piezoelectric energy harvesting and storage from motions of the heart, lung, and diaphragm. *Proc. Natl Acad. Sci. USA* **111**, 1927–1932 (2014).
- Dagdeviren, C. et al. Recent progress in flexible and stretchable piezoelectric devices for mechanical energy harvesting, sensing and actuation. *Extreme Mech. Lett.* **9**, 269–281 (2016).
- Dagdeviren, C. The future of bionic dynamos. *Science* **354**, 1109 (2016).
- Mostafalu, P. & Sonkusale, S. Flexible and transparent gastric battery: energy harvesting from gastric acid for endoscopy application. *Biosens. Bioelectron.* **54**, 292–296 (2014).
- Kim, J. Y. et al. Self-deployable current sources fabricated from edible materials. *J. Mater. Chem. B* **1**, 3781–3788 (2013).
- Persano, L. et al. High performance, flexible piezoelectric devices based on aligned arrays of nanofibers of poly(vinylidene fluoride-co-trifluoroethylene). *Nat. Commun.* **4**, 1633 (2013).
- Persano, L., Dagdeviren, C., Marrucio, C., De Lorenzis, L. & Pisignano, D. Cooperativity in the enhanced piezoelectric response of polymer nanowires. *Adv. Mater.* **26**, 7574–7580 (2014).
- Dagdeviren, C. et al. Transient, biocompatible electronics and energy harvesters based on ZnO. *Small* **9**, 3398–3404 (2013).
- Sirohi, J. & Chopra, I. Fundamental understanding of piezoelectric strain sensors. *J. Intell. Mater. Syst. Struct.* **11**, 246–257 (2000).
- Yong, Y. K., Fleming, A. J. & Moheimani, S. O. A novel piezoelectric strain sensor for simultaneous damping and tracking control of a high-speed nanopositioner. *IEEE/ASME Trans. Mechatron.* **18**, 1113–1121 (2013).
- Shi, Y., & Dagdeviren, C., Rogers, J. A., Gao, C. F. & Huang, Y. An analytic model for skin modulus measurement via conformal piezoelectric systems. *J. Appl. Mech. T. ASME* **82**, 091007 (2015).
- Su, Y., Li, S., Li, R. & Dagdeviren, C. Splitting of neutral mechanical plane of conformal, multilayer piezoelectric mechanical energy harvester. *Appl. Phys. Lett.* **107**, 041905 (2015).
- Dagdeviren, C. et al. Conformal piezoelectric systems for clinical and experimental characterization of soft tissue biomechanics. *Nat. Mater.* **14**, 728–736 (2015).
- Dagdeviren, C. et al. Conformable amplified lead zirconate titanate sensors with enhanced piezoelectric response for cutaneous pressure monitoring. *Nat. Commun.* **5**, 4496 (2014).
- Famm, K., Litt, B., Tracey, K. J., Boyden, E. S. & Slaus, M. Drug discovery: a jump-start for electroceuticals. *Nature* **496**, 159–161 (2013).
- Yang, S. et al. Thermally resistant UV-curable epoxy-siloxane hybrid materials for light emitting diode (LED) encapsulation. *J. Mater. Chem.* **22**, 8874–8880 (2012).
- Yagnamurthy, S. N. *Electromechanical Behavior of PZT Thin Film Composites for RF-MEMS*. Masters Thesis, Univ. Illinois at Urbana Champaign (2009).
- Su, Y. J., Quian, C. F., Zhao, M. H. & Zhang, T. Y. Microbridge testing of silicon oxide/silicon nitride bilayer films deposited on silicon wafers. *Acta Materialia* **48**, 4901–4915 (2000).
- Sharpe, W. et al. Strain measurements of silicon dioxide microspecimens by digital imaging processing. *Exp. Mech.* **47**, 649–658 (2007).
- Bellinger, A. M. et al. Oral, ultra-long-lasting drug delivery: application toward malaria elimination goals. *Sci. Transl. Med.* **8**, 365 (2016).
- Poeggel, S. et al. Optical fibre pressure sensors in medical applications. *Sensors* **15**, 17115–17148 (2015).
- Merritt, J. S. & Weinhaus, F. The pressure curve for a rubber balloon. *Am. J. Phys.* **46**, 976–977 (1978).
- Yu, L., Kim, B. J. & Meng, E. Chronically implanted pressure sensors: challenges and state of the field. *Sensors* **14**, 20620–20644 (2014).
- Bures, J. et al. Small intestinal bacterial overgrowth syndrome. *World J. Gastroenterol.* **16**, 2978–2990 (2010).
- Beyerlein, L. et al. Correlation between symptoms developed after the oral ingestion of 50 g lactose and results of hydrogen breath testing for lactose intolerance. *Aliment. Pharmacol. Ther.* **27**, 659–665 (2008).

33. Nadeau, P. et al. Prolonged energy harvesting for ingestible devices. *Nat. Biomed. Eng.* **1**, 0022 (2017).
34. Yeo, W.-H. et al. Multifunctional epidermal electronics printed directly onto the skin. *Adv. Mater.* **25**, 2773–2778 (2013).
35. Holzapfel, G. A. *Nonlinear Solid Mechanics* (John Wiley & Sons, Chichester, 2000).
36. Overvelde, J. T. B., Kloek, T., D'haen, J. J. A. & Bertoldi, K. Amplifying the response of soft actuators by harnessing snap-through instabilities. *Proc. Natl Acad. Sci. USA* **112**, 10863–10868 (2015).
37. Jones, R. M. *Mechanics of Composite Materials* (Taylor & Francis Group, 1998).

Acknowledgements

We thank J. Haupt and M. Jamiel for help with the in vivo swine work. We thank Y.-A. Lee for assistance with the SEM. We thank the Hope Babette Tang Histology Facility at the Koch Institute at MIT for the histology work and consultation. We also thank the MIT Microsystems Technology Laboratories and MIT Microscopy Core Facility. C.D. thanks the late G. Caliskanoglu for useful suggestions on the device design. This work was funded in part by a postdoctoral fellowship from the Swiss National Foundation (to T.v.E.), National Institutes of Health grant EB-000244, the Max Planck Research Award (Award Ltr Dtd. 2/11/08), the Alexander von Humboldt-Stiftung Foundation (to R.L.) and the Division of Gastroenterology, Brigham and Women's Hospital (to G.T.).

Author contributions

C.D. designed and fabricated the PZT GI-S. C.D. and G.T. designed the in vitro, ex vivo and in vivo experiments. T.v.E. performed the cell culture study and studied the biocompatibility of the PZT GI-S. C.D., P.J., T.B. and Z.W. designed an in vitro setup to simulate stomach behaviour and conducted in vitro trials of PZT GI-S. F.J. performed ABAQUS/Standard for finite element modelling. C.D., S.S., C.C. and L.B. designed and conducted the ex vivo studies. C.D., P.J., S.M., J.C., A.H. and G.T. performed in vivo evaluations of the GI-S in Yorkshire swine models. All authors discussed and interpreted the results, and wrote and edited the paper.

Competing interests

The authors declare no competing financial interests.

Additional information

Supplementary information is available for this paper at <https://doi.org/10.1038/s41551-017-0140-7>.

Reprints and permissions information is available at www.nature.com/reprints.

Correspondence and requests for materials should be addressed to C.D. or G.T.

Publisher's note: Springer Nature remains neutral with regard to jurisdictional claims in published maps and institutional affiliations.